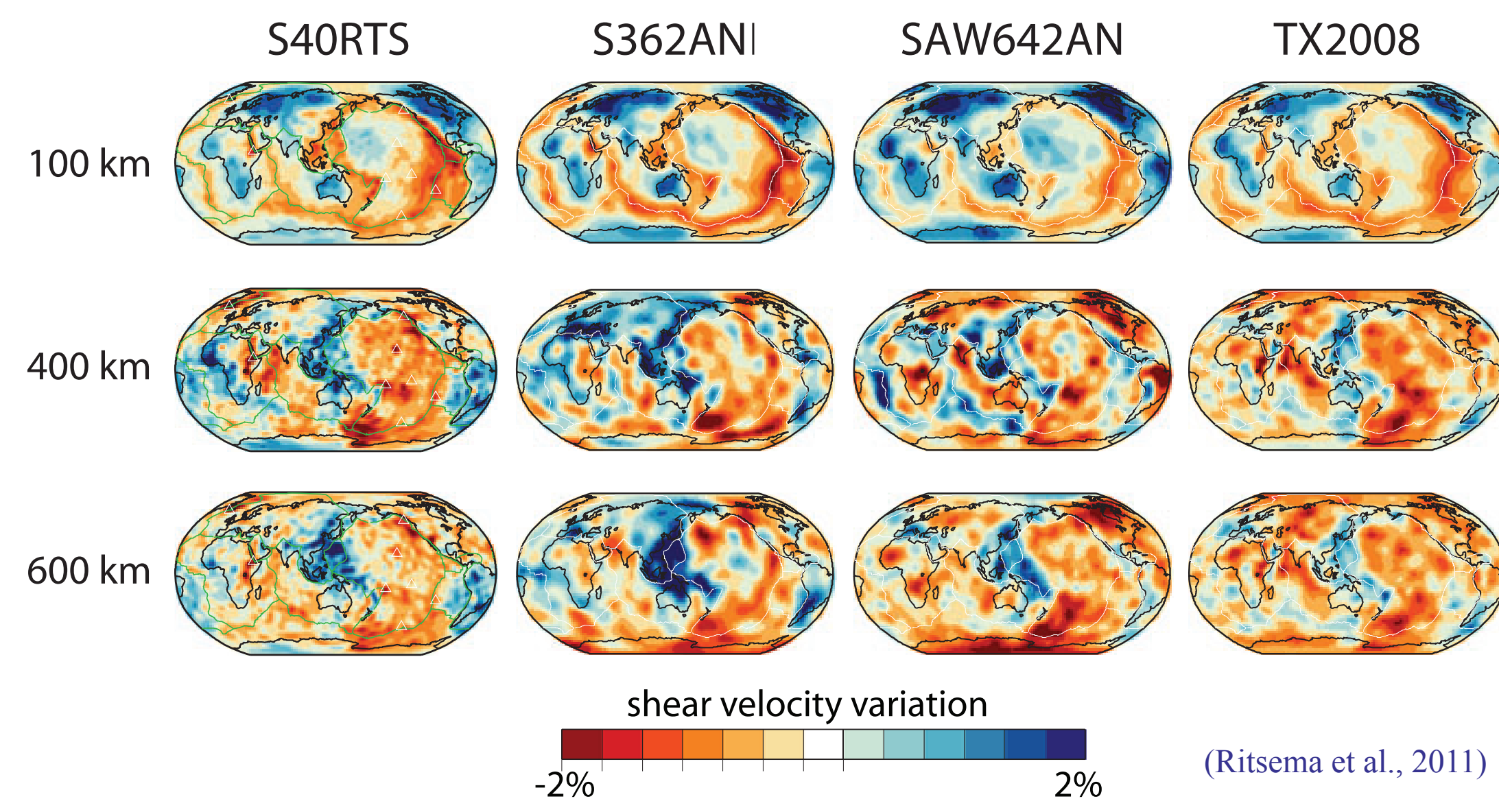


1. Motivation

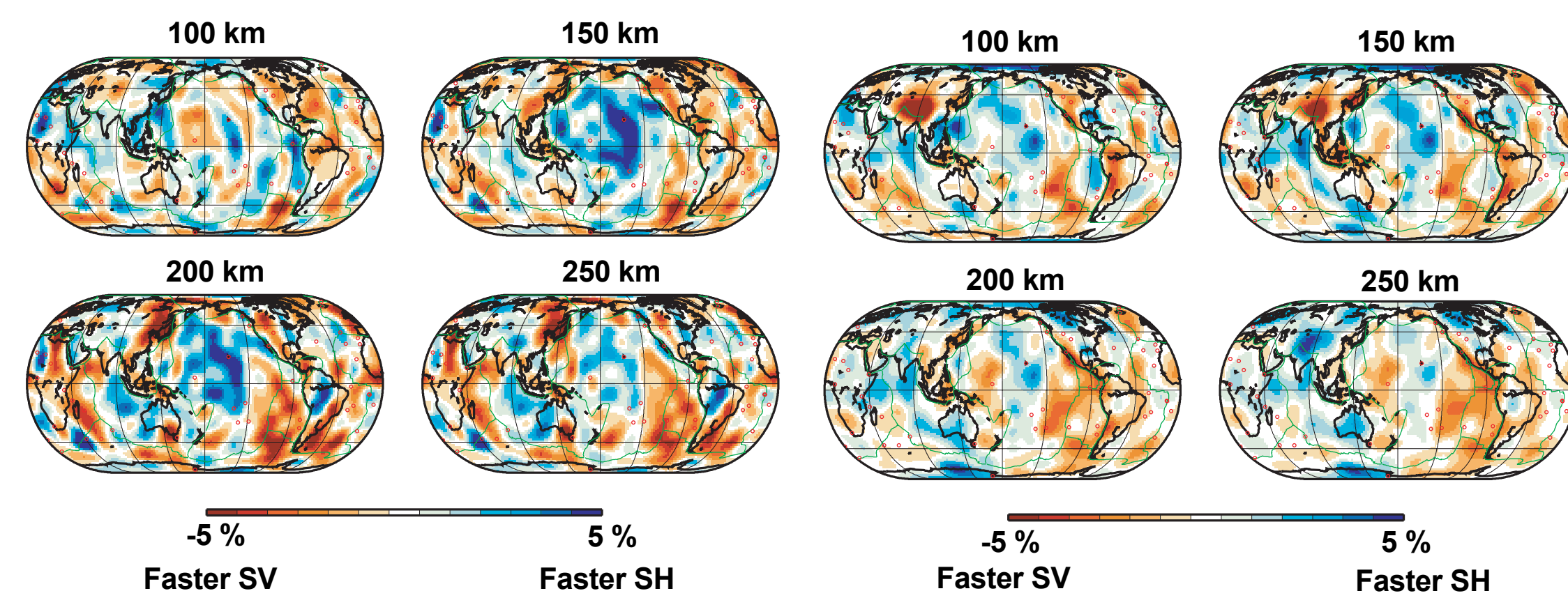
Global Isotropic S-velocity Models



$$\xi = \frac{V_{SH}^2}{V_{SV}^2}$$

S362ANI (Kustowski et al., 2008)

SAW642ANb (Panning et al., 2010)



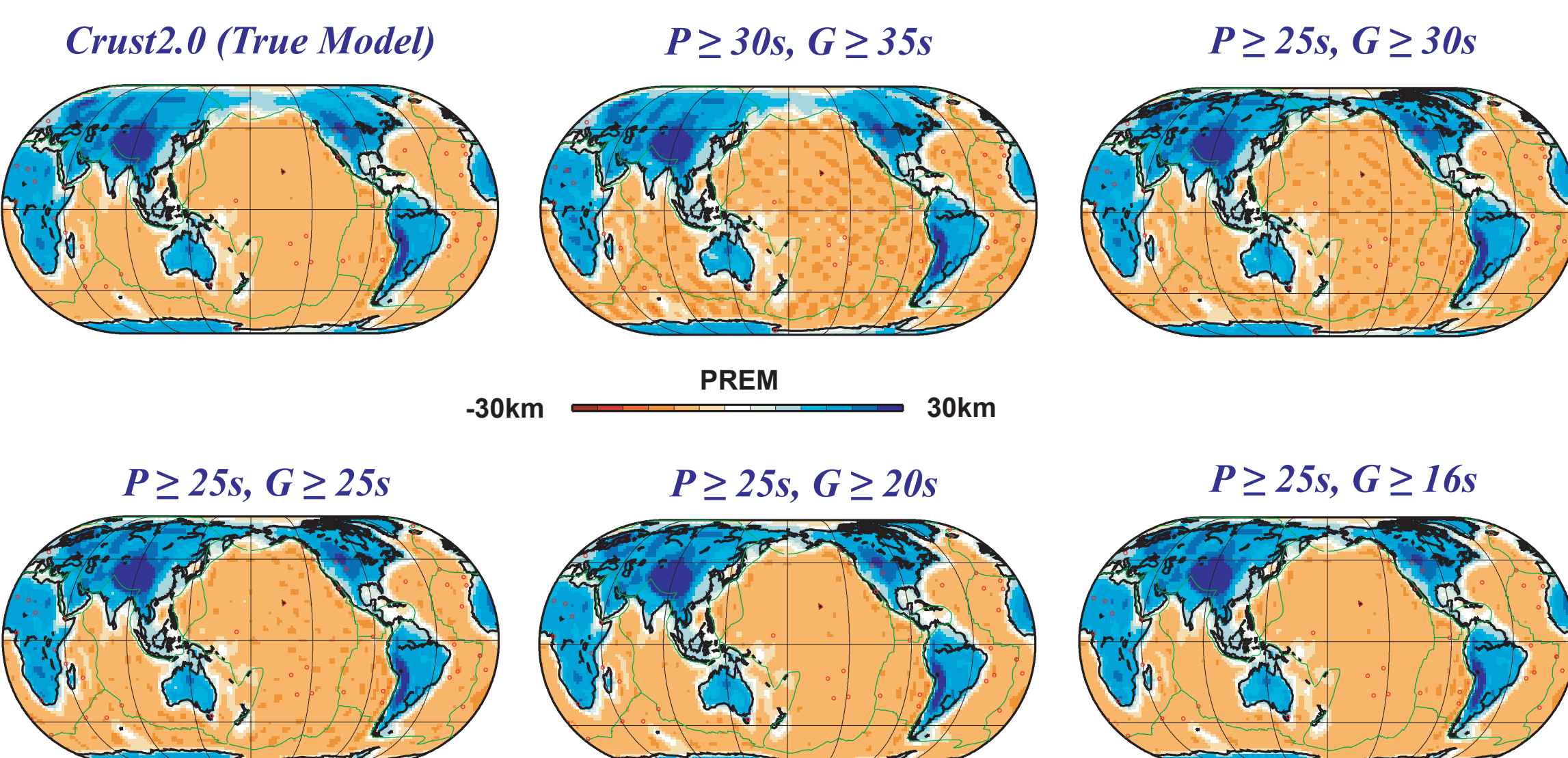
Although various global isotropic S-velocity models built with different parameterizations, damping schemes and datasets are amazingly consistent one another at least in the upper mantle or for low harmonic degrees (Becker and Boschi, 2002), we haven't reached such a consensus on global anisotropic models.

For example, two anisotropic models above show significant differences from each other. SAW642ANb shows faster SV (red) beneath Tibet at 100 km, which is not as strong as the model in S362ANI. On the other hand, S362ANI presents faster SV (red) along the subduction zones in western Pacific and beneath eastern Africa, which are not shown in SAW642ANb.

Effect of Crust

Ferreira et al. (2010) reported that the effect on data misfit of using different crust models shows difference of as large as 2%. On the other hand, data misfit reduction of around 1% is obtained when lateral variations in radial anisotropy are considered. This small misfit reduction is comparable to or smaller than the misfit difference due to different crustal corrections, and this may explain why it is hard to obtain robust radially anisotropic model.

Resolution Tests for Crust



2. Data and Approaches Used in This Study

To constrain radial anisotropy better than previous studies, we are going to incorporate as many data as possible. A computationally efficient way to do this is to adopt great-circle approximation (GCA) in our inversion, which is analogous to ray theory in body wave tomography. We have assembled phase velocity data (P) with overtones and group velocity data (G) from several published studies into an archive of 55 million measurements.

Data (P/G)	Spheroidal mode	Minor arc	Major arc	Toroidal mode	Minor arc	Major arc
E97 (P: Ekström et al., 1997)	Fundamental mode (35-300s)	276,812		Fundamental mode (35-300s)	161,568	
E11 (P: Ekström, 2011)	Fundamental mode (25-250s)	2,548,680		Fundamental mode (35-250s)	661,215	
R04 (P: Ritsema et al., 2004)	Fundamental mode (37.6-374s)	2,693,926		Fundamental mode (37.6-375s)	256,574	
	1 st overtone (37.5-274s)	223,672		1 st overtone (37.5-200s)	64,861	
	2 nd overtone (37.6-365s)	193,919		2 nd overtone (37.5-114s)	20,679	
	3 rd overtone (37.5-203s)	169,908		3 rd overtone (37.6-78s)	9,438	
	4 th overtone (37.5-78s)	129,505				
	5 th overtone (37.5-62s)	68,282				
V08 (P: Visser et al., 2008)	Fundamental mode (35.1-175s)	1,018,048		Fundamental mode (35.1-174s)	722,864	
	1 st overtone (35.1-173s)	864,560		1 st overtone (35.1-177s)	557,744	
	2 nd overtone (35-149s)	786,855		2 nd overtone (35-115s)	412,152	
	3 rd overtone (35-88s)	536,382		3 rd overtone (35.1-79s)	241,020	
	4 th overtone (35.1-62s)	324,848		4 th overtone (35.1-63s)	120,520	
	5 th overtone (35.1-56s)	221,459		5 th overtone (35.1-56s)	59,598	
RL98 (G: Ritzwoller and Levshin, 1998)	Fundamental mode (16-150s)	1,083,328		Fundamental mode (16-100s)	539,147	
	Fundamental mode(v, 37.6-374s)	13,202,786	2,712,997	Fundamental mode(h, 37.6-374s)		
R11 (P: Ritsema et al., 2011)	Fundamental mode(v, 37.6-374s)	3,717,227	428,978	Fundamental mode(h, 37.6-374s)		
	1 st overtone (v, 37.5-274s, 40-)	991,490	649,581	1 st overtone (h, 37.5-274s, 78-)		
	1 st overtone (h, 37.5-274s, 78-)	39,901	24,882			
	2 nd overtone (v, 37.6-365s)	840,796	687,202	Fundamental mode (37.6-375s)	5,244,236	1,436,275
	2 nd overtone (h, 37.6-326s, 88-365s)	96,887	194,607	1 st overtone (37.5-269s, -382s)	1,594,217	664,977
	3 rd overtone (v, 37.5-99s, -233s)	723,823	357,529	2 nd overtone (37.5-151s, -324s)	493,383	218,386
	3 rd overtone (h, 56-273s, 62-324s)	171,253	294,631	3 rd overtone (37.6-101s, -206s)	230,714	125,758
	4 th overtone (v, 37.5-69s, -130s)	474,706	246,553	4 th overtone (37.6-69s, -151s)	104,108	96,198
	4 th overtone (h, 43-149s, 47-233s)	381,723	550,806	5 th overtone (37.5-56s)	57,561	
	5 th overtone (v, 37.5-51s, 37.5-284s)	168,052	208,208			
	5 th overtone (h, 37.5-115s, 37.5-284s)	484,836	626,806			
6 th overtone (v, 78-132s)	0	13,561				
6 th overtone (h, 37.6-78s, 37.6-132s)	415,264	587,934				
Sum		32,978,719	7,584,275		11,551,599	2,541,594

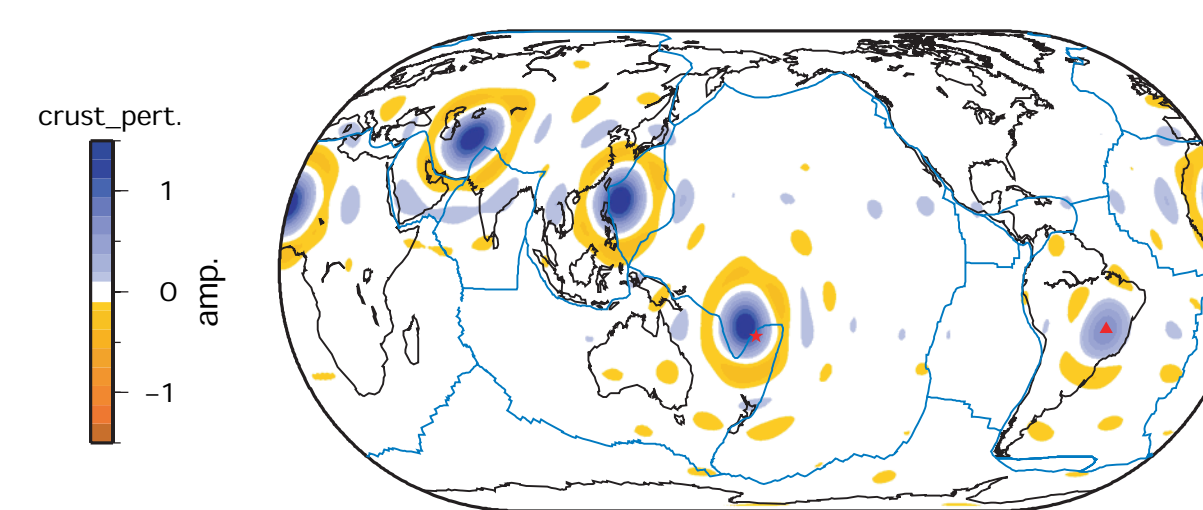
Considering Crustal Thickness Perturbation

GCA has an advantage that exact crustal correction is possible for each cell point with the corresponding 1D model. But 3D effect such as focussing and defocussing is not taken into account. Furthermore, CRUST2.0 widely used for crustal correction is not accurate enough even for long period data. To consider these problems in crustal correction, we adopt crustal thickness perturbation as a model parameter, which may absorb the uncorrected crustal structure by CRUST2.0. To better constrain crustal thickness, we incorporate short period group velocity data down to 16s.

Travel Time Data

Phase	Number	Component
S	172,738	T
SS	114,270	T
SSS	25,097	T
ScS	8,517	T
ScS2	13,590	T
ScS3	8,025	T
SKS	32,309	R
SKKS	8,839	R
sS	20,238	T
sSS	9,770	T
sSSS	2,763	T
sScS	1,606	T
sScS2	3,483	T
sSKS	2,465	R
SSm	654	T, major arc
SSSm	3,227	T, major arc
SSSSm	1,340	T, major arc
sSSm	50	T, major arc
sSSSs	974	T, major arc
sSSSSm	1,003	T, major arc
Total:	433,663	

Crustal thickness kernel for sSSSS



To constrain the lower mantle, we incorporate travel time data used for constructing S40RTS (Ritsema et al., 2011).

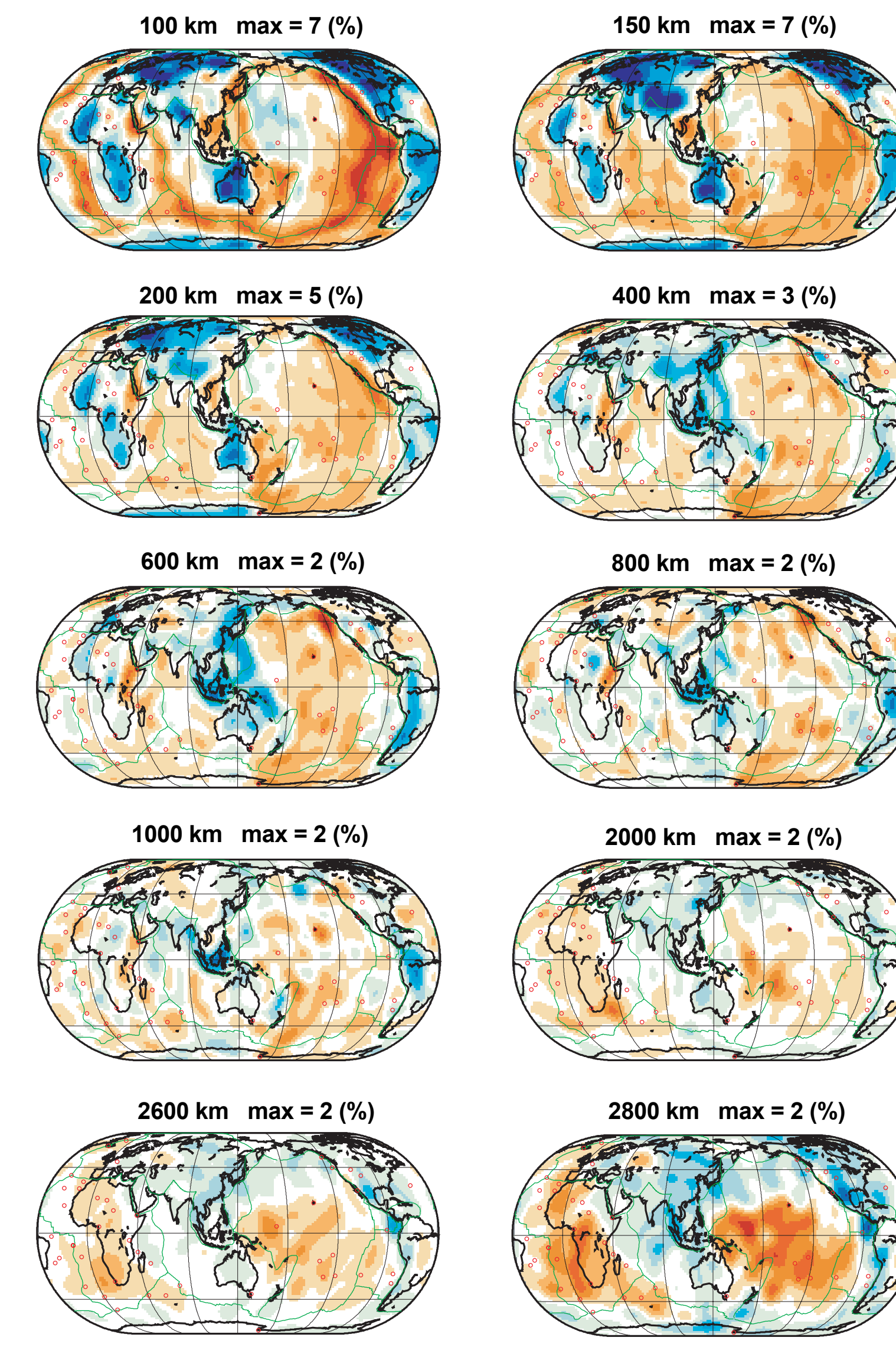
Dominant paths in individual dataset can bias inversion results, so we set a weight to each wave path by the number of similar event-station pairs to suppress biases due to dominant paths in individual data as well as to make a balance among various datasets.



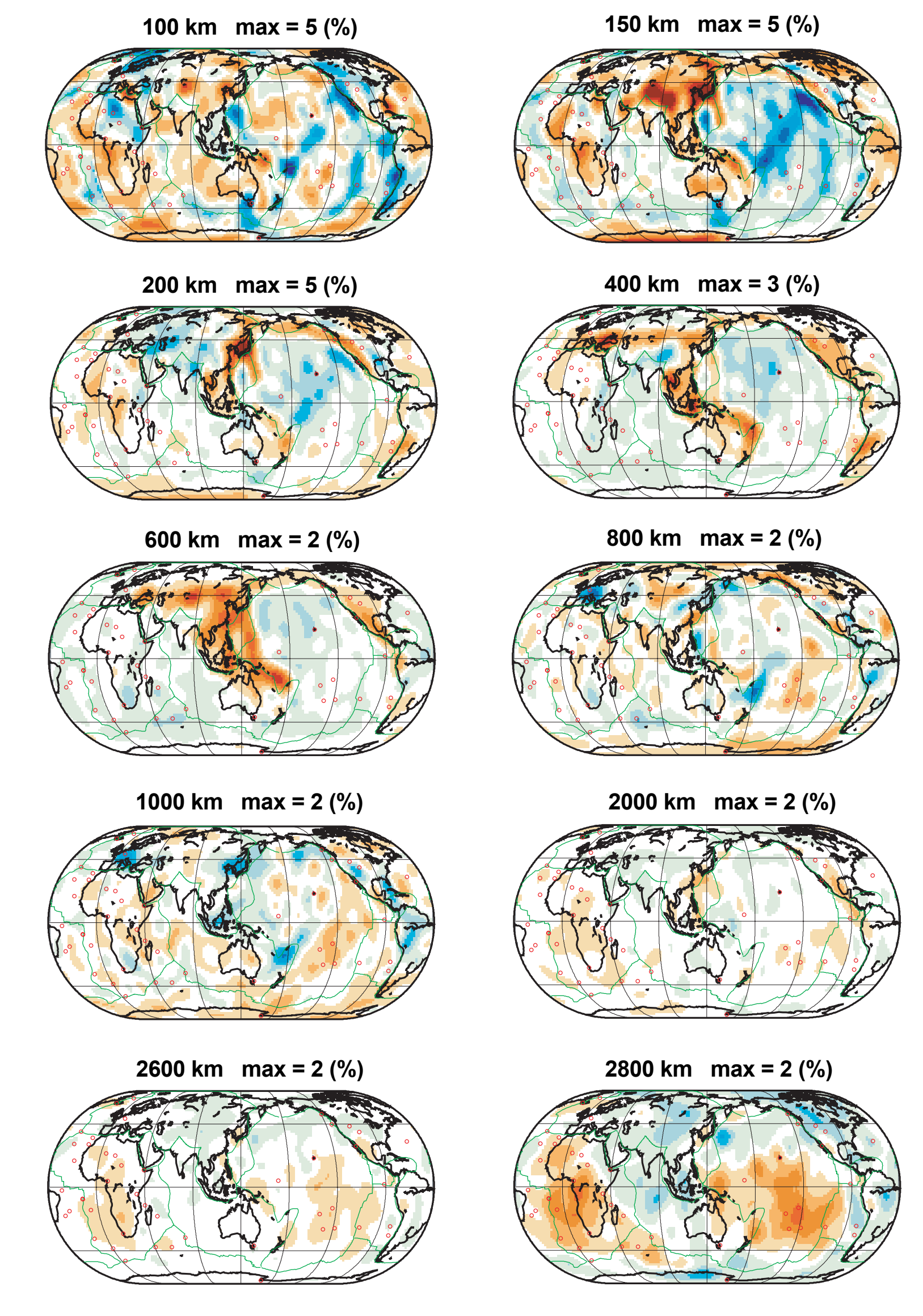
3. Results

(lmax=20, 21 depth splines, effective # of parameters=3500)

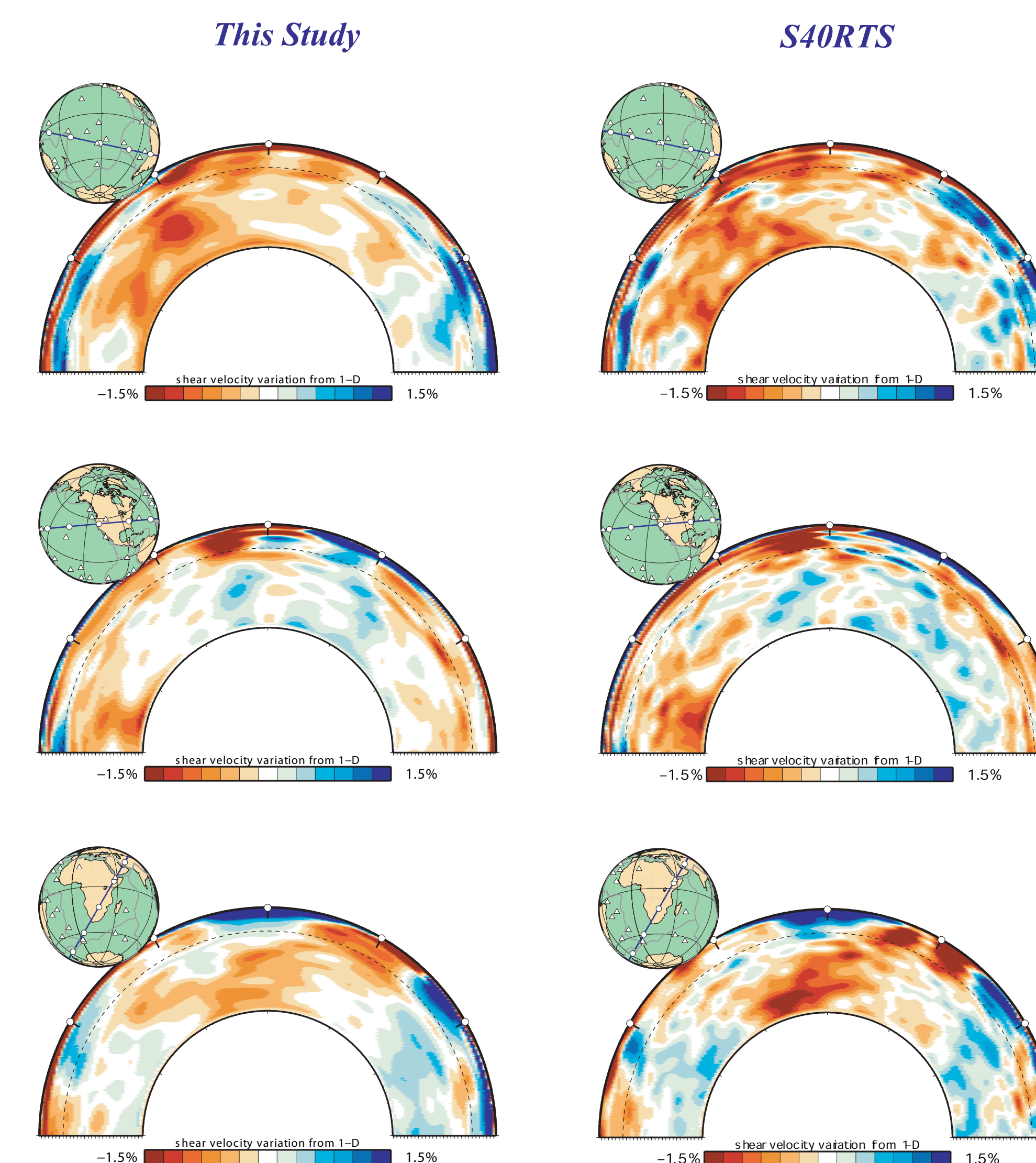
Isotropic Models



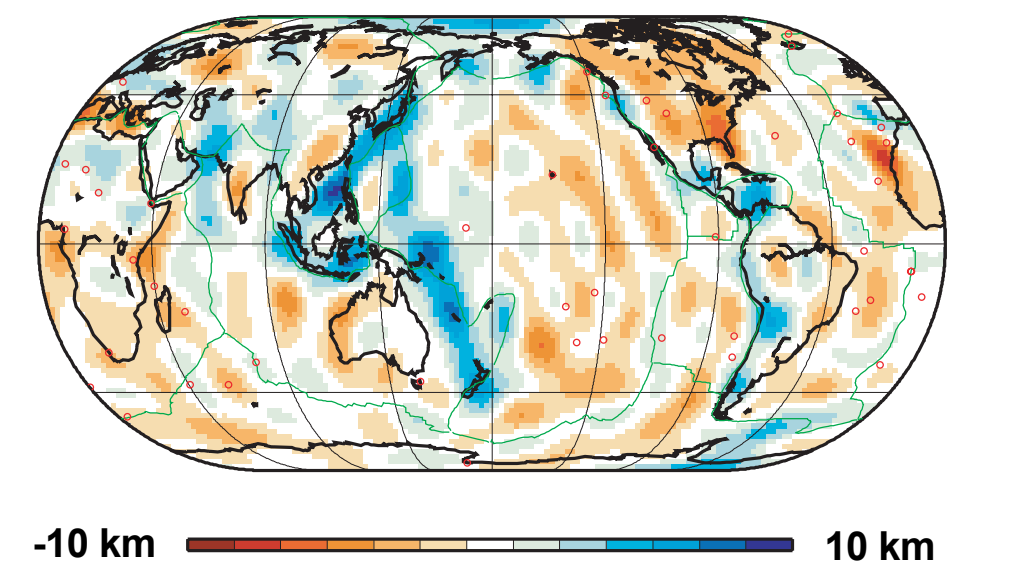
Anisotropic Models



Cross Sections of Isotropic Models



Crustal Thickness Perturbation from CRUST2.0



4. Conclusions

The various datasets used are highly complementary, allowing us to achieve good resolution in both isotropic and anisotropic structure throughout the mantle.

Crustal correction with CRUST2.0 is not accurate enough. Adopting crustal thickness perturbation as a model parameter can be a solution to separate uncorrected part of crust from mantle velocity structure.

Significant misfit reduction of 7~8% for surface wave data is achieved with use of crustal thickness perturbation and lateral variation of radial anisotropy in our study comparing to isotropic inversion given the same effective number of model parameters, which may imply that radial anisotropy can be constrained beyond the error range.